Improved Analytical Model for a Proximity Coupled Microstrip Patch Antenna (PC-MSPA)

Nim Ccoillo-Ramos, *Student Member, IEEE*, Nafati Aboserwal, *Member, IEEE*, Zeeshan Qamar, *Member, IEEE*, and Jorge L. Salazar-Cerreno, *Senior Member, IEEE*

***Abstract*—This paper presents an accurate full analytical model to assess the impedance response of a proximity-coupled microstrip patch antenna (PC-MSPA). An improved formulation of the patch resonant frequency is used to calculate the quality factor, resonant resistance, and the feeding circuit parameters of the antenna. The proposed model also assesses the PC-MSPA impedance response while considering the fabrication constraints. For the validation of the proposed model, at first, the antennas are simulated for S-, C- and X-bands. Then, two prototypes are fabricated and measured. The proposed model predicts the antenna resonant frequency and impedance bandwidth with less than 1% error.**

***Index Terms*—Analytical modeling, equivalent circuit, impedance response, microstrip antenna, proximity coupling.**

I. Introduction

Since the development of the microstrip patch antenna in the twentieth century [1], [2], it has been widely used due to its low profile, ease of fabrication, and easy integration with microwave circuits [3]. However, this antenna usually presents challenges when the bandwidth requirement is larger than 10%. Different strategies have been proposed in the literature to deal with these limitations [4], [5]. The feeding technique of an MSPA plays an important role in its frequency response. The probe-fed technique [6] produces a highly inductive impedance response limiting the bandwidth to a few percent. The aperture coupling feeding [7] produces low spurious radiation due to the isolation between the feed and the patch. The proximity coupling feeding [8] is more likely to behave with capacitive impedance and wider bandwidth.

Antenna modeling through analytical approaches allows accurate estimations of the antenna behavior, e.g. the bandwidth [9]. The first documented design guidelines and analytical models appeared in the early 80s [6], [10], [11]. Diverse models for MSPAs with different feeding techniques were developed decades ago, beginning with the transmission line and the cavity models [7]. Rigorous studies and analyses for rectangular and circular MSPAs employing probe-fed and inset-fed techniques were performed in [6] and [12], providing an equivalent RLC circuit for the patch. In [13], an analysis of the aperture-coupled MSPA based on integral equations and Green's functions was presented, constituting an initial step in the development of circuit-based models. A detailed investigation of an electromagnetically coupled rectangular patch antenna was presented in [14], proposing an equivalent circuit based on the reciprocity theory. More recent models for the resonant frequency have been developed for a circular patch antenna [15] with less than 2% of error. For rectangular patches, existing models [16]–[18] predict the resonant frequency with errors between 1.5% and 5.5% for substrate thicknesses in the range between $0.003\lambda_0$ and $0.05\lambda_0$.

Although there are models for microstrip patch antennas, limited models on the PC-MSPA are published. The accuracy of the PC-MSPA are compromised due to the complexity of the feeding mechanism and interaction with the patch voltage and current distribution. The impedance of the PC-MSPA cannot be directly determined under the end of the transmission line position unless the fringing fields around the edge and the variable stripline characteristic impedance are considered. In [8], a numerical circuit model for the PC-MSPA was obtained. The model consists of a capacitor in series with an RLC resonator, and the behavior of the feeding was predominantly capacitive when the overlapping section of the feed was low compared to the patch length. In [19], a circuit model for a circular PC-MSPA with a hybrid feed of an L-strip line was developed. In this model, the total capacitance resulted from the direct capacitances between the overlapping portions of the feed and the plates above and below it, as well as the fringing capacitances between the open ends of the feed and of the patch and the ground plane. This is the nearest approach to the work proposed in this paper, where the L-strip portion of the feeding in the original work can be suppressed to obtain the antenna geometry used in this work. However, this model is not accurate. Limitations in the accuracy of the resonant frequency and resonant resistance in microstrip patches significantly affect the accuracy of the impedance response model in PC-MSPAs. This paper proposes an improved model based on an electric equivalent circuit to predict the impedance response of a two-layer single-material PC-MSPA.

This model includes the formulation of the patch resonant frequency, quality factor, and resonant resistance, as well as the feeding circuit elements. A mathematical and physical background on microstrip antennas are provided in Section II. Then, the proposed model of a PC-MSPA and its mathematical formulation are presented in Section III. In Section IV, four antenna prototypes are designed, fabricated and tested to validate the proposed model and their results are discussed in Section V. Finally, the conclusion of this work is presented in Section VI.

N. Ccoillo, N. Aboserwal, Z. Qamar and J. Salazar, are with the Phased Array Antenna Research and Development (PAARD) group, the Advanced Radar Research Center (ARRC) and the Department of Electrical and Computer Engineering, The University of Oklahoma, Norman, OK, 73019 USA. Website: http://www.ou-arrc-paard.com

Manuscript received April 14, 2021

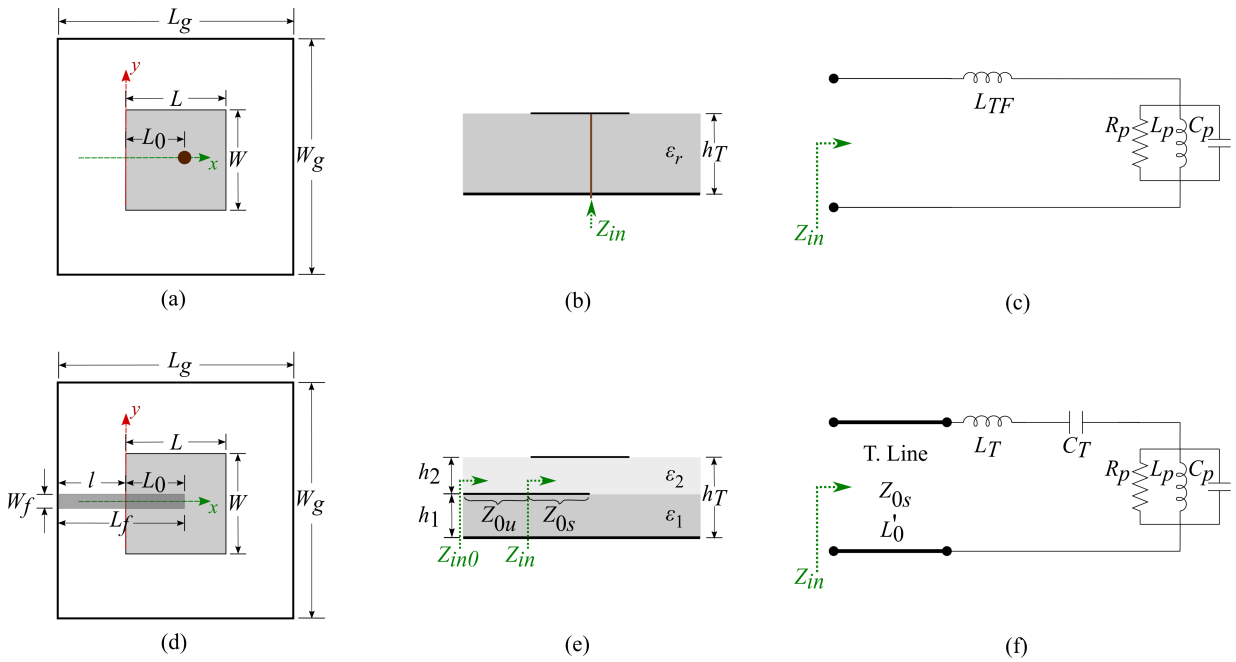

Fig. 1: Geometry and equivalent circuit model of the PC-MSPA. (a) Top view. (b) Side view. (c) Equivalent circuit model.

II. Background and Theory for the PC-MSPA

The geometry of a PC-MSPA is shown in Fig. 1a,b, having two substrate layers, the patch, the ground plane, and a feeding transmission line between the layers. The bottom substrate (h_1, ε_1) supports the feed at the top and the ground plane on the bottom, while the top substrate (h_2, ε_2) supports the patch on the top. A substrate thickness ratio can be defined as $r_h = h_2/h_1$. For this study, both substrates are of the same material and the same thickness, i.e. $\varepsilon_1 = \varepsilon_2 = \varepsilon_r$ and $r_h = 1$. The patch length, which determines the resonant frequency (f_{0p}), is set to $L \approx \lambda_g/2$. To make the impedance response stable, the ground plane size is $L_g = W_g = 2\lambda_0$. The transmission line with length L_f, used as a feed, has a section L_0 that overlaps the patch. The position $x = 0$ in Fig. 1a is the reference location where Z_{in} is obtained.

From a circuit perspective, the MSPA can be modeled as an RLC parallel resonator in series with an equivalent circuit of the feed section. The equivalent circuit model of the PC-MSPA is shown in Fig. 1c, where the RLC circuit and the LC circuit account for the patch and the proximity-coupled microstrip line, respectively [6]. The patch RLC circuit is fully defined by the resonant frequency f_{0p} [15], [18], the quality factor Q_p [6], [16], and the resonant resistance R_p [16], [18]. The value of R_p is related to the maximum resonant resistance R_{pM} and the feed position L_0. Using the antenna dimensions of the geometry shown Fig. 1a,b, the parameters f_{0p}, Q_p and R_{pM} can be obtained.

Considering the patch as a microstrip transmission line of width W, over a substrate with a thickness of h_T and a relative permittivity of ε_r, the effective relative permittivity ε_{re} can be calculated as [18]:

$$\varepsilon_{re} = (\varepsilon_r + 1)/(2) + (\varepsilon_r - 1)/(2)\big(1 + 10h_T/W\big)^{-0.5} \quad (1)$$

However, the more accurate effective relative permittivity ε_{rep} used in the design procedure has been empirically determined to be as in (2). It is worth noting that (2) has been slightly modified from the original formulation of [17] to get more accurate resonant frequency.

$$\varepsilon_{rep} = 0.5\varepsilon_r + 0.5\varepsilon_{re}, \quad (2)$$

On the other hand, the fringing fields, which are due to the finite dimensions of the patch, are counted through an small extension ΔL [20]. A precise expression of ΔL is listed in (3) where $\zeta_1, \zeta_2, \zeta_3, \zeta_4$ and ζ_5 are also defined in [20].

$$\Delta L = h_T\ \zeta_1\zeta_3\zeta_5/\zeta_4, \quad (3)$$

Thus, the resonant frequency of the RLC resonator is:

$$f_{0p} = \frac{c_0}{2L_e\sqrt{\varepsilon_{rep}}}, \quad (4)$$

where c_0 is the free-space speed of light and L_e is the patch effective length $L_e = L + 2\Delta L$. Hence, the wavelength (λ_{0p}) and the wavenumber (k_{0p}) at resonance are:

$$\lambda_{0p} = c_0/f_{0p} \quad (5)$$

$$k_{0p} = 2\pi/\lambda_{0p} \quad (6)$$

The resonator quality factor Q_p [16] can be calculated considering the losses of the dielectric, the conductor, the radiation and the surface waves through Q_d, Q_c, Q_{rad} and Q_{sw}, and it is given by

$$\begin{aligned} Q_p &= [Q_d^{-1} + Q_c^{-1} + (Q_{rad}^{-1} + Q_{sw}^{-1})]^{-1} \\ &= \left[\delta_d + \frac{1}{h_T\sqrt{\pi f_{0p}\mu\sigma}} + \frac{16}{3}\frac{pc_1}{\varepsilon_r}\frac{h_T}{\lambda_{0p}}\frac{W_e}{L_e}\frac{1}{e_r^{hed}}\right]^{-1}, \end{aligned} \quad (7)$$

where δ_d, μ and σ are the substrate tangent-loss, substrate permeability, and copper conductivity. The values of p, c_1, and e_r^{hed} are defined in [16].

This article has been accepted for publication in a future issue of this journal, but has not been fully edited. Content may change prior to final publication. Citation information: DOI 10.1109/TAP.2021.3082570, IEEE Transactions on Antennas and Propagation

The resonant resistance R_p [16] is related to its maximum value R_{pM} and the effective feed position $L_{0e} = L_0 + \Delta L$ along the patch effective length L_e, and R_{pM} is expressed as:

$$R_{pM} = (4/\pi)(\mu_r \eta_0) Q_p (L_e/W_e)(h_T/\lambda_{0p}) \quad (8)$$

$$R_p = R_{pM} \cos^2\left(\pi \frac{L_{0e}}{L_e}\right) = R_{pM} \cos^2\left(\pi \frac{L_0 + \Delta L}{L + 2\Delta L}\right) \quad (9)$$

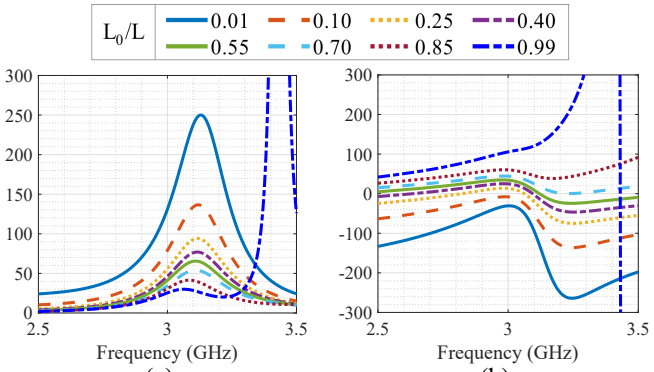

Fig. 2: Variations of impedance response of a PC-MSPA with different feed lengths. (a) Real part. (b) Imaginary part.

The components of the parallel RLC circuit [16] for a microstrip patch are expressed as:

$$R_p = R_{pM} \cos^2(\pi L_{0e}/L_e) \quad (10)$$

$$L_p = \frac{R_p}{2\pi f_{0p} Q_p} \quad (11)$$

$$C_p = \frac{Q_p}{2\pi f_{0p} R_p} \quad (12)$$

Then, the total impedance Z_p of the parallel RLC circuit of the patch can be calculated using (13).

$$Z_p = 1/(1/R_p + 1/j\omega L_p + j\omega C_p) \quad (13)$$

A. Problem and proposed solution

Although antenna models for the PC-MSPAs are available in the literature, and some of them have become progressively more sophisticated, there are still limitations in predicting the impedance behavior for different lengths of the feed. To illustrate these limitations, Fig. 2 shows the impedance behavior of a PC-MSPA along different overlap ratios ($l_{0n} = L_0/L$) ($0 < l_{0n} < 1$) using antenna Design 1 (Table I, Section IV). The limitations on the model can be observed when exciting the patch underneath its center ($l_{0n} = 0.5$) which produces an all-zero input impedance as $R_p = 0$ according to (10), which is not true as observed in Fig. 2. The curves in Fig. 2a show a decaying resonant resistance as the feed becomes longer. This implies an alternative profile of the radiation resistance that does not necessarily correspond with the cosine-squared profile of (10). The patch resonant frequency and quality factor change slightly across the feed lengths, especially when $0.25 < l_{0n} < 0.75$. Also, very high resistances and shifts in the patch resonant frequency are observed when $l_{0n} > 0.90$. Using lower overlap ratios, it is shown in Fig. 2b that the antenna response is predominantly capacitive, as already observed in [8]. On the other hand, for high overlap ratios, the response tends to be more inductive. No phase rotation is perceived in the response while $l_{0n} < 0.75$, indicating that the increase of the reactance is produced by larger capacitances and inductances. If only the capacitances are considered, then the response would be limited because the maximum reactance value would be the half of the resonant resistance, which is not true especially when $l_{0n} > 0.70$.

In summary, the behavior of a PC-MSPA can be dependent on the overlap ratio as follows:

- Short overlaps ($l_{0n} < 0.25$): The impedance response has capacitive reactance, and the resonant resistance dramatically changes with slight variations of the feed length. An equivalent capacitor in series with the RLC resonator fits very well in this case.
- Moderate overlaps ($0.25 \leq l_{0n} \leq 0.75$): The impedance response has capacitive and inductive reactance. The resonant resistance decreases as the feed becomes longer with less sensitivity. An LC circuit in series with the patch RLC resonator fits very well in this overlap range.
- Large overlaps ($l_{0n} > 0.75$): The patch resonant frequency gets shifted and open-circuit impedances appear at the upper frequencies of the interval analysis as a phase rotation is produced. An equivalent transmission line in series with the LC-RLC series is required to better model the behavior of the PC-MSPA.

Therefore, the proposed solution consists of a new model to obtain the impedance of a PC-MSPA with feed lengths in the range of moderate overlaps. The model is composed of a set of equations for the patch resonator and the feeding inductance and capacitance, integrating them in a hybrid model structure of a transmission line in series with a LC-RLC circuit.

III. Proposed Model For The PC-MSPA

In this section, a new model for a PC-MSPA is presented. The model is divided into three parts: a patch RLC resonator, a feeding circuit, and a feeding equivalent transmission line. Notice that for moderate overlaps, on which this work focuses, the equivalent transmission line can be ignored. An equivalent circuit of the proposed model is presented in Fig. 1c. The input impedance of the PC-MSPA Z_{in} is given by

$$Z_{in} = Z_p + Z_{feed} = \mathrm{Re}(Z_p) + j\mathrm{Im}(Z_p + Z_{feed}), \quad (14)$$

This means that the real part of Z_{in} only depends on the patch resonator, while the imaginary part depends on both the patch resonator and the feeding.

A. Patch RLC resonator

The parameters f_{0p}, Q_p, and R_{pM} can be calculated considering the average relative permittivity of the two substrates ε_r, the total thickness $h_T = h_1 + h_2$, and the length of the patch L. For R_p, the length of overlapping section of the feed L_0 is also required for the calculation. Because the coupling mechanism in the PC-MSPA depends on the substrates thickness ratio, the

expressions (4), (7), (8) and (9) of f_{0p}, Q_p, R_{pM} and R_p of Section II need to be reformulated.

The RLC resonant frequency in PC-MSPAs (f_{0p}) has been observed to shift upwards with respect to the RLC resonant frequency of the same patch but with probe feeding. To consider this shift and use (4), a factor F_{f0} is applied as expressed in (15). In order to avoid any confusion, the RLC resonant frequency calculated in (4) is renamed to f_{0r}, thus the corresponding wavelength (5) is also renamed to λ_{0r}. Then, f_{0p} is expressed as

$$f_{0p} = f_{0r}F_{f0} = f_{0r}(F_0 + (h_T/\lambda_{0r} - 0.005)F_1), \quad (15)$$

where $F_0 = 1.02 - 0.045/\sqrt{\varepsilon_r}$ and $F_1 = (0.7376/r_h + 0.4754)/\sqrt{\varepsilon_r}$. The result of (15), obtained by curve fitting techniques [21], has an error less than 1% with simulated data of square PC-MSPA designs, and over the range $\varepsilon_r \in [1.7; 3.66]$, $r_h \in [0.75; 1.25]$ and $h_T \leq 0.1\lambda_{0r}/\sqrt{\varepsilon_r}$. After f_{0p} is calculated, (5) - (6) can be used to obtain λ_{0p} and k_{0p} which will be used to get Q_p and R_p.

Following the patch cavity model, its effective length L_e can be calculated using (16), where f_{0p} has been calculated in (15). Hence, the value of ΔL for PC-MSPAs can be rewritten as in (17)

$$L_e = \frac{c_0}{2f_{0p}\sqrt{\varepsilon_{rep}}} \quad (16)$$

$$\Delta L = 0.5(L_e - L) \quad (17)$$

The RLC quality factor in a patch is a function of the resonant frequency, the relative permittivity, and the patch effective dimensions (L_e, W_e). By comparison with simulated data, it was observed that a value of W_e as in (18) enables prediction of the quality factor of the square PC-MSPA with errors less than 10%. It is important to indicate that this value of W_e only represents a mathematical estimate.

$$W_e = W + 2\Delta W \approx W + 2(0.25\Delta L) \quad (18)$$

Consequently, the RLC quality factor of PC-MSPAs can be calculated using (7) considering the resonant frequency f_{0p} of (15) and the effective dimensions of (16) and (18).

The RLC resonant resistance R_p of PC-MSPAs can be rewritten as in (20). The value of R_{pM} expressed in (19) was obtained from (9) using $L_0 = 0$ and a square patch, and it can be calculated using:

$$R_{pM} = \frac{4}{\pi}(\mu_r\eta_0)Q_p\Big(\frac{h_T}{\lambda_{0p}}\Big)\cos^2\Big(\frac{\pi\Delta L}{L + 2\Delta L}\Big) \quad (19)$$

$$R_p = R_{pM}F_{Rp} \quad (20)$$

The shape curve F_{Rp} is expressed in (21) for short and moderate overlaps assuming $h_1 = h_2$.

$$F_{Rp} = 32.38\big(1 - l_{0n}^{0.005}\big) + 0.14 \quad (21)$$

A more accurate expression of F_{Rp} that includes the influence of the thickness ratio $r_h = h_2/h_1$ is:

$$F_{Rp} = Ae^{-p_1 l_{0n}} + (1 - A)e^{-p_2 l_{0n}}, \quad (22)$$

where

$$A = \sqrt{r_h}(-0.66e^{-97.13\frac{h_T}{\lambda_{0r}}} + 0.74e^{-4.505\frac{h_T}{\lambda_{0r}}}) \quad (23)$$

$$p_1 = \frac{1.544}{\frac{h_T}{\lambda_{0r}} + 0.01456} \quad (24)$$

$$p_2 = r_h^{0.75}\Big[1.456 - 1.698e^{-32.18\frac{h_T}{\lambda_{0r}}}\Big] \quad (25)$$

These terms, obtained by curve fitting techniques with non-linear regression [21], provide a fast-decay exponential shape dictated by p_1 and a slow-decay shape, dictated by p_2. Typical values of p_1 are around several tens, while p_2 is a value between 0.5 and 1.5. Therefore, for moderate overlap ratios, the first term of (22) can be ignored to calculate F_{Rp}.

B. Feeding circuit

The feeding structure can be modeled as an in-series LC circuit as pictured in Fig. 1c. The variation of the feeding inductance and capacitance (L_T, C_T) are shown in Fig. 3b,c as a function of the overlapping ratio l_{0n}. These values were obtained by selecting the combination (L_T, C_T) that produced the least impedance error between the model and simulated results of Z_{in}. Hence, L_T and C_T can be expressed as in (30) and (31) for moderate overlap ratios as demonstrated below.

First, for $\varepsilon_{r1} = 2.2$, $\mu_{r1} = 1$, $f_{0p1} = 2.945$ GHz,

$$L_{T1} = A_1e^{4.551l_{0n}} \quad (26)$$

$$C_{T1} = B_1(l_{0n} - 0.4534)^2 + B_3, \quad (27)$$

where $A_1 = 0.1587$, $B_1 = -11$, $B_3 = 1.797$.

Since the patch is designed to have a length of $L = \lambda_g/2$ and the overlapping length of the feeding L_0 depends on L to have l_{0n} constant, then (26) and (27) can be generalized as:

$$L_T = L_{T1}\frac{f_{0p1}\sqrt{\mu_{r1}}}{f_{0p}\sqrt{\mu_r}} \quad (28)$$

$$C_T = C_{T1}\frac{f_{0p1}\sqrt{\varepsilon_{r1}}}{f_{0p}\sqrt{\varepsilon_r}} \quad (29)$$

Thus, replacing (28) and (29) in (26) - (27):

$$L_T = \frac{A_{1s}}{f_{0p}\sqrt{\mu_r}}e^{4.551l_{0n}} \quad (30)$$

$$C_T = \frac{1}{f_{0p}\sqrt{\varepsilon_r}}\big[B_{1s}(l_{0n} - 0.4534)^2 + B_{3s}\big], \quad (31)$$

where $A_{1s} = 0.4674$, $B_{1s} = -48.05$, $B_{3s} = 7.85$, f_{0p} is in GHz, L_T is in nH, and C_T is in pF.

As observed in (30) - (31), the feeding equivalent inductance is negligible at short overlaps, but it becomes significant as the overlap ratio increases. Also, the equivalent capacitance increases up to a maximum around $l_{0n} = 0.45$ and decreases as the overlap ratio increases.

C. Feeding equivalent transmission line

For short and moderate overlaps, the transmission line of Fig.1c can be ignored, since the response does not get shifted and the input reactance increases almost linearly with the frequency, i.e. having an inductance. However, for large overlaps, an equivalent transmission line of length $L_0^{'}$ needs to be added to the LC feed circuit model, where $L_0^{'} \leq L_0$. Physically, this line may be due to the proximity between the open ends and the non-planar feature of the structure which is more

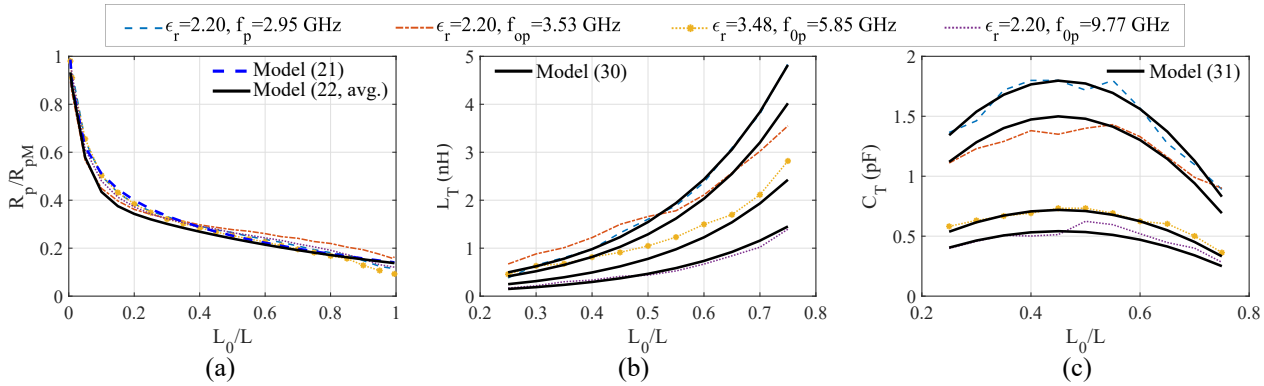

Fig. 3: Model parameters vs. overlap ratio. (a) Normalized radiation resistance (R_p/R_{pM}). (b) Feeding inductance (L_T). (c) Feeding capacitance (C_T).

noticeable at large overlaps. Because the overlapping portion of the feeding is between the patch and the ground plane, the equivalent transmission line takes the form of a stripline (with impedance Z_{0s}) [22] instead of an embedded microstrip line (with impedance Z_{0u}) [23], [24]. Notice that the equivalent resonant resistance may be less than that plotted in Fig. 3a when including this equivalent transmission line. The feeding inductance and capacitance may not continue following the pattern pictured in Fig. 3b,c, as $l_{0n} \to 1$, Q_p may decrease and R_p may get close to zero.

IV. Validation of the Proposed Model

The proposed model is validated with simulated and measured results of the impedance of PC-MSPAs designed at 3 GHz, 3.5 GHz, 5.4 GHz and 9.4 GHz. The proposed antenna design is shown in Fig. 1a,b and the dimensions of the proposed designs are listed in Table I. In order to show the generalized capability of the proposed model, the proposed designs are different from the ones used to get the model equations. Different overlap ratios l_{0n} are used to show the model assessment, regardless of the maximum return loss that the antenna gets at f_0. An assessment in both Z_{in} and S_{11} parameters is presented. Furthermore, the radiation patterns are evaluated and discussed at the end of this section.

The model performance using the de-embedded wave port in HFSS (ideal condition) is illustrated in Fig. 5 through a comparison between modeled and simulated responses of the input impedance and the S_{11} parameter. The results were obtained considering an ideal waveport in the simulated designs and de-embedding the port from the position $x = -(L_f - L_0)$ to $x = 0$. In addition, the values of the patch RLC resonator parameters are compared in Table III between the modeled and simulated values.

The assessment of the model performance using a coaxial probe feed (real condition) is performed through the comparison between the modeling, simulations, and measurements of antenna designs 2 and 3 of Table I. Even though the antenna fabrication was intended to replicate the same specifications during the fabrication process, an air gap h_a and a slight movement of the patch p_m occurred. The effect of fabrication imperfections is illustrated in Fig. 4. This effect needs to be considered in the model to have more accurate results.

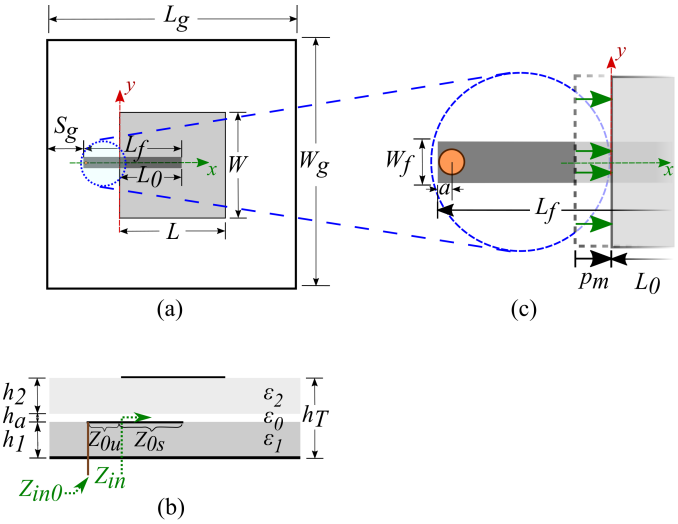

Fig. 4: Geometry and dimensions of the fabricated PC-MSPA. (a) Top view. (b) Side view, with air gap h_a between the substrates. (c) The patch movement p_m representation.

TABLE I: Antennas' design specifications.

Specifications	Units	D1 [9]	D2 [8]	D3 (this work)	D4 (this work)
f_o	GHz	3.0	3.5	5.4	9.4
$\varepsilon_1, \varepsilon_2$	-	2.2	2.2	2.2	2.2
h_1, h_2	mm	3.175	1.575	1.575	0.787
L, W	mm	27.7	26.1	16.6	9.65
l_{0n}	-	0.25	0.50	0.70	0.60
L_f	mm	93.08	90	59.32	32.72
W_f	mm	9.00	4.55	4.55	2.30
L_g, W_g	mm	200	180	112	63.5
h_T	λ_0	0.063	0.037	0.057	0.049

TABLE II: Fabricated antennas' specifications.

Specifications		Units	D2 [8]	D3 (this work)
Avg. relative permittivity	ε'_r	-	1.954	2.086
Estimated air gap	h_a	mm	0.37	0.15
Measured patch size	L, W	mm	26.3± 0.1	16.55 ± 0.1
Estimated patch movement	p_m	mm	-2.00	0.85
Effective overlap ratio	l'_{0n}	-	0.576	0.751
Space to antenna border	S_g	mm	65.71	40.60
Feeding length	L_f	mm	24.29	18.71

The air gap h_a is included in the model by reformulating the effective thickness used for the patch substrate h'_2 (32) instead

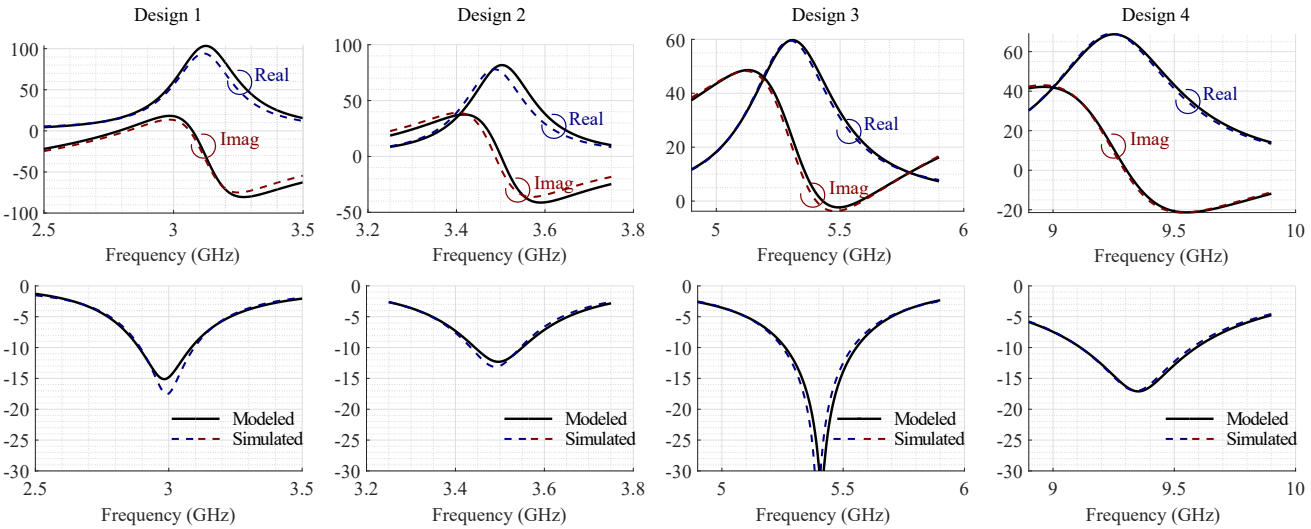

Fig. 5: Comparison between modeled and simulated impedance responses $Z_{in}(\Omega)$ (top row) and S_{11} (dB) (bottom row) plots.

of the physical thickness h_2. Thus, the thickness ratio and the total thickness are also affected by h_2' in (33) - (34).

$$h_2' = h_2 + h_a \tag{32}$$

$$r_h' = h_2'/h_1 \tag{33}$$

$$h_T = h_2' + h_1 \tag{34}$$

Moreover, the average relative permittivity [25] ε_r' is calculated as:

$$\frac{h_T}{\varepsilon_r'} = \sum_{i=1}^{n} \frac{h_i}{\varepsilon_{r,i}} \tag{35}$$

The patch movement along the $x-$axis is also considered in the model, especially to determine the overlap ratio, which is a meaningful parameter needed to accurately determine the resonant resistance R_p. In Fig. 4c, this shift is indicated as p_m, which is positive if the patch is moved as indicated in the arrows, and negative if moved in the opposite direction. The inclusion of p_m in the model is done with an effective overlap ratio of l_{0n}' calculated from the expected overlap ratio l_{0n} as:

$$l_{0n}' = (l_{0n}L - p_m)/L \tag{36}$$

The described dimensions are listed in Table II. The specifications not mentioned were already listed in Table I.

TABLE III: A comparison between modeled and simulated patch parameters (RLC equivalent circuit).

	Source	D1 [9]	Error (%)	D2 [8]	Error (%)	D3 (this work)	Error (%)	D4 (this work)	Error (%)
f_{0p}	Model	3.125	-	3.503	-	5.308	-	9.252	-
	Simul.	3.120	0.15	3.490	0.37	5.300	0.15	9.240	0.13
Q_p	Model	10.46	-	19.53	-	12.60	-	14.57	-
	Simul.	10.75	2.70	20	2.35	13	3.08	14.95	2.54
R_p	Model	103	-	81.7	-	59.7	-	68.8	-
	Simul.	94.1	9.88	78.0	4.78	59.5	0.28	69.1	0.39

"-" means *no data*. The errors consider the simulation data as references.

The modeled impedance Z_{in} from the reference position at $x = 0$ is transformed to the measurement position as Z_{in0}, as pictured in Fig. 4b, located under the ground plane and connected through a 50Ω coaxial cable and a probe.

TABLE IV: A comparison between modeled, simulated and measured values of the impedance bandwidth and resonant frequencies.

Parameters		D2 [8]	Error (%)	D3 (this work)	Error (%)
Resonant frequency (f_0)	Modeled	3.655	-	5.517	-
	Simulated	3.648	0.18	5.509	0.15
	Measured	3.650	0.12	5.508	0.16
Minimum frequency in bandwidth (f_l)	Modeled	3.578	-	5.400	-
	Simulated	3.565	0.36	5.378	0.41
	Measured	3.561	0.48	5.374	0.48
Maximum frequency in bandwidth (f_h)	Modeled	3.731	-	5.628	-
	Simul.	3.729	0.05	5.629	0.02
	Measured	3.728	0.07	5.632	0.07
Impedance bandwidth (BW)	Modeled	4.19	-	4.13	-
	Simulated	4.50%	0.31	4.56%	0.42
	Measured	4.58%	0.40	4.68%	0.55

"-" means *no data*. The errors consider the simulation and measurement data as references.

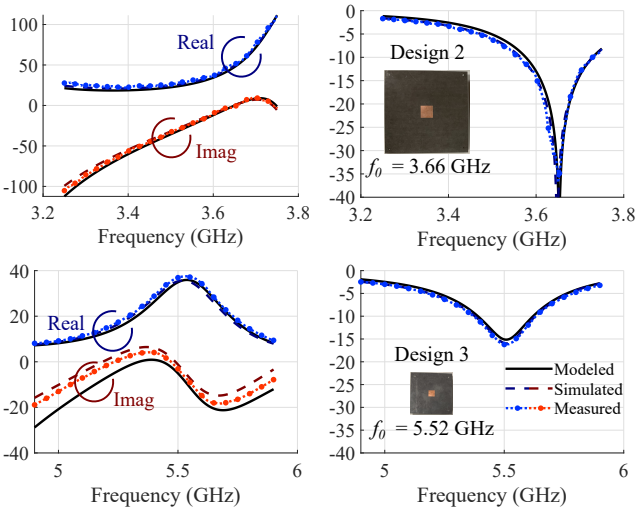

Fig. 6: Comparison between modeled, simulated and measured impedance responses (Ω) and S_{11} parameter (dB) for the fabricated antennas Design 2 and Design 3.

Hence, Fig. 6 provides a comparison between modeled, simulated, and measured values of the impedance and S_{11} parameter, when the antennas include a coaxial connector

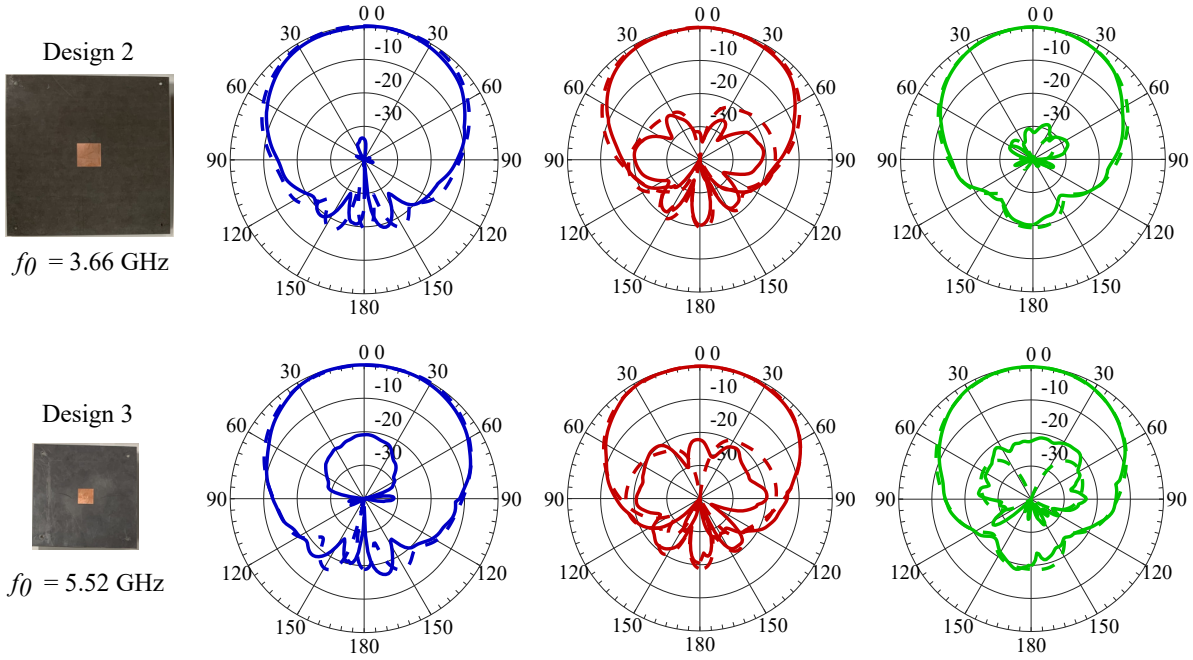

Fig. 7: Normalized co- and cross-polarized radiation patterns in the $E-$, $D-$ and $H-$planes (from left to right). Simulated (dashed line) and measured (solid line) radiation patterns of the design antennas Design 2 and Design 3.

under the specific location ($x = -(L_f - L_0)$). This 50Ω connector has an inner and outer radius of 0.65 mm and 2.10 mm, respectively, and the dielectric is Teflon-based material ($\varepsilon_r = 2.0$). Table IV lists a comparison between measured, simulated, and modeled resonant frequencies f_0, in-bandwidth minimum f_l and maximum f_h frequencies, and the impedance bandwidth of the antenna designs from the S_{11} parameter data.

A. PC-MSPA radiation patterns

The expressions of the far-field radiation patterns of a PC-MSPA over a theoretical infinite ground plane are given in (37) - (38) using the patch dimensions and substrate thickness [26].

$$E_\theta \propto -\frac{\cos\phi \cos X \operatorname{sinc} Y \operatorname{tanc} Z}{1 + j\tan(Z)} \tag{37}$$

$$E_\phi \propto \frac{\cos\theta \sin\phi \cos X \operatorname{sinc} Y \operatorname{tanc} Z}{1 + j\tan(Z)} \tag{38}$$

where $X = kL/2 \sin\theta\cos\phi$, $Y = kW/2 \sin\theta \sin\phi$, $Z = kH_T \cos\theta$, $\operatorname{sinc}\alpha = (\sin\alpha)/\alpha$ and $\operatorname{tanc}\alpha = (\tan\alpha)/\alpha$ are defined in [26].

The fields produced by the PC-MSPA can be obtained using the equivalent radiating slots using the patch cavity model [18]. The length of each slot is represented by the width of the patch (W). The separation between slots is dictated by the patch length (L). In the previous expressions, the term $\operatorname{sinc} Z$ can be ignored, since $\sin(Z)$ can be approximated to Z when very thin substrates are used. The modified 2nd Ludwig's definition of the cross polarization is used [27], [28]. According to [28], there are two variants of this definition, depending on the feeding orientation. The variant 2-I is used for patches fed along the x-axis, as pictured in Fig. 4. The simulated and measured radiation patterns of antenna designs 2 and 3 are shown in Fig. 7, where a good agreement between them is found for the E-, H- and D-planes.

V. Discussion

The plots in Fig. 5 show great agreement between modeled and simulated impedance responses when the model is validated using the de-embedded wave port in HFSS (ideal condition). A frequency shift is more perceptible in D2 as it has the lowest thickness. A resonant resistance shift is observed in D1, which is the electrically thickest model. Comparing the modeled and simulated real parts of the design responses, very low errors are observed. Errors are slightly more perceptible in D2, primarily as a consequence of the frequency shift. The S_{11} plots of the second row of Fig. 5 show that the -10 dB bandwidth is predicted very well, as is the resonant frequency of the four antenna designs, although some difference in the coupling level due to calculation errors in the R_p is observed in D1. It is important to note that the inductance L_T has a critical role in the accuracy of the feed reactance, especially in D3, which has a reactance response above $j0$ Ω. This would not have been possible if the model considered only a capacitor, as seen in the third column of Fig. 5.

The comparison of patch RLC parameters listed in Table III shows that the resonant frequency f_{0p} presents errors less than 0.5%. This high accuracy is necessary because it is used as part of the required variables to calculate the other two parameters (Q_p, R_p) and the feeding parameters (L_T, C_T). The quality factor presented errors less than 3.5%, not showing dependency of these errors on substrate thickness. However,

the resonant resistance can be more accurately determined for antennas with thinner substrates.

Model performance using a coaxial probe (real condition) also presents good agreement, even though these cases require additional transmission line transformations. As seen in Fig. 6, the impedance response, and the reflection coefficient are very well predicted. The model required impedance transformations to convert the impedance response at $x = 0$ to the actual port location. A slight difference is noticed, but a good match in the resonant frequency and the bandwidth is obtained.

The model is able to predict the resonant frequency with errors less than 0.2%. It is important to indicate that the measurement uncertainty was also counted in the model computation, as the patch length directly affects f_{0p}. Considering the frequency interval where $|S_{11}| < -10$ dB, the model is able to predict the impedance bandwidth with error less than 1%, as listed in the last rows of Table IV.

VI. Conclusion

An accurate mathematical model of the PC-MSPA has been proposed and validated. The relative position of the feed along the patch was defined by the ratio l_{0n}. This ratio was used to develop an exponential-based equation for the resonant resistance, as well as a frequency-based equation for the feeding capacitance and inductance. The proposed equivalent circuit and equations allowed a simple but accurate model to be built for the PC-MSPA. The model was validated with antenna designs on S-, C- and X-bands. In all cases, the feed and patch had a moderate overlap ratio. Thus, the calculated -10 dB frequency interval and bandwidth presented errors less than 1% when comparing simulated and measured results, despite the differences found in the coupling level at frequencies near the resonance. The differences in the coupling level may be decreased by adjusting the equation of the patch resonant resistance. Also, the far-field radiation patterns presented high symmetry and moderately high cross-polarization isolation levels, showing that the PC-MSPA model can be useful to build a design with a highly accurate predicted impedance response.

Acknowledgment

The authors are thankful to the Advanced Radar Research Center (ARRC) of The University of Oklahoma for providing the facilities needed to perform this research. They also would like to thank the Phased Array Antenna Research and Development group (PAARD) members for the discussions and positive feedback. This research was sponsor by the U.S. Dept. of Commerce, National Oceanic and Atmospheric Administration (DOC-NOAA).

References

[1] A. G. Deschamps, "Microstrip microwave antennas," *Third USAF Symposium on Antennas*, 1953.

[2] H. Gutton and G. Baissinot, "Flat aerial for ultra high frequencies," *French Patent No. 703 113*, 1955.

[3] Y. Liu, L.-M. Si, M. Wei, P. Yan, P. Yang, H. Lu, C. Zheng, Y. Yuan, J. Mou, X. Lv, and H. Sun, "Some recent developments of microstrip antenna," 2012.

[4] N. Liu, S. Gao, L. Zhu, L. Ji, L. Yang, and H. Zheng, "Low-profile microstrip patch antenna with simultaneous enhanced bandwidth, beamwidth, and cross-polarisation under dual resonance," *IET Microwaves, Antennas Propagation*, vol. 14, no. 5, pp. 360–365, 2020.

[5] D. Sun, Z. Zhang, and X. Yan, "A wideband dual-polarized patch antenna," in *Proceedings of 2014 3rd Asia-Pacific Conference on Antennas and Propagation*, July 2014, pp. 84–86.

[6] K. Carver and J. Mink, "Microstrip antenna technology," *IEEE Trans. Antennas Propag.*, vol. 29, no. 1, pp. 2–24, January 1981.

[7] R. Garg, P. Bhartia, I. Bahl, and A. Ittipiboon, *Microstrip Antenna Design Handbook*. Artech House, 2001.

[8] D. M. Pozar and B. Kaufman, "Increasing the bandwidth of a microstrip antenna by proximity coupling," *Electronics letters*, vol. 23, no. 8, pp. 368–369, 1987.

[9] N. Aboserwal, N. R. Ccoillo Ramos, Z. Qamar, and J. L. Salazar-Cerreno, "An accurate analytical model to calculate the impedance bandwidth of a proximity coupled microstrip patch antenna (PC-MSPA)," *IEEE Access*, vol. 8, pp. 41 784–41 793, 2020.

[10] J. James, P. Hall, C. Wood, and A. Henderson, "Some recent developments in microstrip antenna design," *IEEE Trans. Antennas Propag.*, vol. 29, no. 1, pp. 124–128, 1981.

[11] G. Splitt and M. Davidovitz, "Guidelines for Design of electromagnetically coupled microstrip patch antennas on two-layer substrate," *IEEE Trans. Antennas Propag.*, vol. 38, no. 7, pp. 1136–1140, 1990.

[12] F. Abboud, J. P. Damiano, and A. Papiernik, "Accurate model for the input impedance of coax-fed rectangular microstrip antenna with and without air gaps," in *6th International Conference on Antennas and Propagation*, 1989, pp. 102–106 vol.1.

[13] P. Sullivan and D. Schaubert, "Analysis of an aperture coupled microstrip antenna," *IEEE Trans. Antennas Propag.*, vol. 34, no. 8, pp. 977–984, 1986.

[14] N. C. Karmakar and A. Bhattacharyya, "Electromagnetically coupled patch antenna- Theoretical and experimental investigations," *Microwave and Optical Technology Letters*, vol. 5, pp. 115–118, Mar. 1992.

[15] D. Guha, "Resonant frequency of circular microstrip antennas With and without air gaps," *IEEE Trans. Antennas Propag.*, vol. 49, no. 1, pp. 55–59, 2001.

[16] D. R. Jackson, S. A. Long, J. T. Williams, and V. B. Davis, "Computer-aided design of rectangular microstrip antennas," in *Advances in microstrip and printed antennas*, ser. Wiley Series in Microwave and Optical Engineering, W. C. K. F. Lee, Ed. New York, NY, USA: John Wiley ans Sons Inc., 1997, ch. 5, pp. 223–272.

[17] D. G. Fang, *Antenna Theory and Microstrip Antennas*. Taylor & Francis group, 2010.

[18] C. A. Balanis, *Antenna Theory: Analysis and Design*. John Wiley & Sons, 2015.

[19] A. K. Singh, R. K. Gangwar, and B. K. Kanaujia, "Bandwidth enhancement of L-probe proximity-fed annular ring microstrip slot antenna," in *6th IEEE/International Conference on Advanced Infocomm Technology (ICAIT)*, July 2013, pp. 195–197.

[20] M. Kirschning, R. H. Jansen, and N. H. L. Koster, "Accurate model for open end effect of microstrip lines," *Electronics Letters*, vol. 17, no. 3, pp. 123–125, 1981.

[21] S. L. Arlinghaus, *Practical Handbook of Curve Fitting*. CRC Press, 1994.

[22] M. K. Hammood, "Impedance of stripline," *Tikrit Journal of Pure Science*, vol. 17, no. 4, pp. 144–147, 2012.

[23] R. Garg, I. Bahl, and M. Bozzi, *Microstrip Lines and Slotlines.* Artech House, 2013.

[24] IPC, *Design guide for high-speed controlled impedance circuit boards*, ser. IPC standard. IPC, 2004.

[25] K. Lee, Fong, and K.-F. Tong, *Microstrip patch antennas*. Singapore: Springer Singapore, 2016, pp. 787–852.

[26] D. Guha and J. Siddiqui, "Computer aided design of microstrip antennas," in *Microstrip and printed antennas: New trends, techniques and applications*, ser. Wiley Series in Microwave and Optical Engineering, Y. A. D. Guha, Ed. West Sussex, UK: John Wiley and Sons Inc., 2010, ch. 2, pp. 35–64.

[27] A. Ludwig, "The Definition of cross polarization," *IEEE Trans. Antennas Propag.*, vol. 21, no. 1, pp. 116–119, January 1973.

[28] N. A. Aboserwal, J. L. Salazar, J. A. Ortiz, J. D. Díaz, C. Fulton, and R. D. Palmer, "Source current polarization impact on the cross-polarization definition of practical antenna elements: Theory and applications," *IEEE Trans. Antennas Propag.*, vol. 66, no. 9, pp. 4391–4406, Sep. 2018.

Nim R. Ccoillo Ramos (S'19) got the B. Sc. and M. Sc. degrees in electronics engineering from Universidad Nacional de Ingenieria, Lima, Peru, in 2016 and 2018, respectively. At the end of his undergraduate studies, he joined the National Institute of Research and Training in Telecommunications, Peru, working in electronics engineering with focus on electromagnetism. During his graduate studies, he worked in X-and-P-band SAR image processing to estimate forest changes in the Amazon, having a six-month stay at the Department of Telecommunications of the State University of Campinas, Brazil. He is currently pursuing the PhD program in electrical and computer engineering at the University of Oklahoma, Norman, USA, researching in electromagnetic antenna modeling for phased arrays in the Advanced Radar Research Center.

Nafati Aboserwal (S'13-M'16) received the B.S. degree in Electrical Engineering from Al-Mergheb University, Alkhoms, Libya, in 2002. He received his M.S. and Ph.D. degrees in Electrical Engineering from Arizona State University, Tempe, AZ, in 2012 and 2014, respectively. In January 2015, he joined the Advanced Radar Research Center (ARRC) and the Department of Electrical and Computer Engineering at The University of Oklahoma (OU), Norman, as a Postdoctoral Research Scientist. Currently he is a Research Associate and a Manager of Far-Field, Near-Field and Environmental Anechoic Chambers at the Radar Innovations Laboratory (RIL). His research interests include EM theory, computational electromagnetics, antennas, and diffraction theory, edge diffraction and discontinuities impact on the array performance. His research also focuses on active high performance phased array antennas for weather radars, higher modes and surface waves characteristics of printed antennas, and high performance dual-polarized microstrip antenna elements with low cross-polarization. Dr. Aboserwal is a member of the IEEE Antennas and Propagation Society.

Zeeshan Qamar (S'11-M'17) received the B.Sc. and M.Sc. degrees in electrical engineering from the COMSATS University, Islamabad, Pakistan, in 2010 and 2013, respectively, and the Ph.D. degree in electronic engineering from the City University of Hong Kong, Hong Kong, in 2017. From Jul. 2010 to Aug. 2013, he was a Research Associate with the Department of Electrical and Computer Engineering, COMSATS University. From Nov. 2017 to Apr. 2018, he was a Postdoctoral Research Associate with the Department of Materials Science and Engineering, City University of Hong Kong. He is currently a Postdoctoral Research Fellow with the Phased Array Antenna Research and Development group (PAARD) and the Advanced Radar Research Center at The University of Oklahoma, Norman, OK, USA. His current research interests include micro/millimeter-wave circuits, material characterization, meta-materials, artificial dielectric layer, antennas and phased arrays, phased array antennas. He is a member of the IEEE Antennas and Propagation Society (AP-S), and a reviewer of various IEEE conferences and journals.

Jorge L. Salazar-Cerreno (S'00-M'12-S'14) received a B.S. In ECE from the University Antenor Orrego, Trujillo, Peru, M.S. degree in ECE from the University of Puerto Rico, Mayagüez (UPRM). In 2011, he received his Ph.D. degree in ECE from the University of Massachusetts, Amherst. His Ph.D. research focused on development of low-cost dual-polarized active phased array antennas (APAA). After graduation, Dr. Salazar-Cerreno was awarded a prestigious National Center for Atmospheric Research (NCAR) Advanced Study Program (ASP) postdoctoral fellowship. He joined the Advanced Radar Research Center (ARRC) at The University of Oklahoma as a research scientist, and became an assistant professor at the School of Electrical and Computer Engineering in August 2015. His research interests include high-performance, broadband antennas for dual-polarized phased array radar applications; array antenna architecture for reconfigurable radar systems; APAA; Tx/Rx modules; radome EM modeling; and millimeter-wave antennas. In 2019, Dr. Salazar was awarded the prestigious William H. Barkow Presidential Professorship from The University of Oklahoma for meeting the highest standards of excellence in scholarship and teaching. Dr. Salazar is a senior member of the IEEE Antennas and Propagation Society (AP-S), and a reviewer of various IEEE and AMS conferences and journals.